Development of Predictive Model based on Medical Image for Prediction of Diagnosis and Treatment Prognosis in Patients with Pulmonary Hypertension

Seongmin Ha

The Graduate School
Yonsei University
Graduate Program
in Biomedical Engineering

Development of Predictive Model based on Medical Image for Prediction of Diagnosis and Treatment Prognosis in Patients with Pulmonary Hypertension

A Dissertation Submitted
to the Graduate Program in Biomedical Engineering
the Graduate School of Yonsei University
in partial fulfillment of the
requirements for the degree of
Doctor of Philosophy in biomedical engineering

Seongmin Ha

June 2024

This certifies that the Dissertation
of Seongmin Ha is approved.

Thesis Supervisor	Hyuk-Jae Chang
Thesis Committee Member	Jae-Hyeong Park
Thesis Committee Member	Eui-Young Choi
Thesis Committee Member	Seungik Baek
Thesis Committee Member	Hyunsoo Yoon

The Graduate School
Yonsei University
June 2024

Acknowledgements

이 논문을 작성하는 동안 많은 분들의 도움이 있었습니다. 이 자리를 빌려 그분들께 진심으로 감사의 마음을 전하고자 합니다.

먼저, 지도교수님이신 장혁재 교수님께 깊은 감사를 드립니다. 교수님의 탁월한 지도와 격려가 없었다면 이 연구를 완성할 수 없었을 것입니다. 연구의 각 단계에서 주신 귀중한 조언과 지도가 큰 도움이 되었습니다. 또한, 심학준 교수님, 유선국 교수님, 백승익 교수님께도 감사의 말씀을 드립니다. 연구 진행 중 많은 도움과 조언을 주셨고, 항상 협력적인 자세로 함께 해주셨습니다. 교수님들의 지원이 없었다면 이 논문을 완성하는 데 많은 어려움이 있었을 것입니다.

연구실 동료 여러분께도 감사드립니다. 함께 연구하면서 많은 지식과 아이디어를 공유할 수 있었습니다. 특히, 밤낮으로 함께 많은 고민을 나눈 영걸, 세근, 현석, 재익, 영택, 도현, 훈, 그리고 후배님들, 언제나 힘이 되는 병환이형, 성희, 그리고 든든한 저희 팀원들 모든 분들께 감사의 말씀을 드립니다. 여러분의 도움과 격려 덕분에 연구를 진행하는 데 큰 힘이 되었습니다.

항상 변함없는 사랑과 지지를 보내주신 어머니, 아버지, 그리고 동생 정아와 함께 이 기쁨을 나누고 싶습니다. 가족의 응원과 격려가 없었다면 이 길을 끝까지 걸어올 수 없었을 것입니다. 또한, 저의 반려자인 서인이에게도 감사의 말씀을 전합니다. 늘 곁에서 힘이 되어주고, 이해해주었기에 이 논문을 완성할 수 있었습니다.

끝으로, 이 논문을 위해 직간접적으로 도움을 주신 모든 분들께 다시 한 번 감사의 말씀을 드립니다. 여러분의 도움과 격려 덕분에 이 논문을 성공적으로 완성할 수 있었으며, 앞으로도 학문에 정진하여 더 나은 연구자가 되도록 노력하겠습니다.

2024 년 6 월
하 성 민

Table of Contents

LIST OF FIGURES

LIST OF TABLES

ABSTRACT

Development of Predictive Model based on Medical Image for Prediction of Diagnosis and Treatment Prognosis in Patients with Pulmonary Hypertension

Pulmonary hypertension (PH) is a condition characterized by elevated pressure in the pulmonary arteries resulting from various pulmonary and cardiac diseases. This elevation in pressure increases the strain on the heart, leading to right ventricular overload and potentially right heart failure, which significantly affects the patient's prognosis.

This study aims to develop a technology that supports non-invasive examinations by deriving hemodynamic computational fluid dynamics (CFD) simulation results from echocardiography and computed tomography (CT) images. These results will be used to develop a deep learning model (DL-CFD). Additionally, a model incorporating the clinical results of echocardiography (eDL-CFD) will be evaluated for validity. By comparing these models with traditional echocardiography methods, the study confirms the potential for clinical use of this combined approach.

Between 2008 and 2019, a retrospective study analyzed 92 patients who underwent right heart catheterization (RHC) for PH assessment, including 75 diagnosed with PH (mPAP > 25 mmHg) and 17 suspected but not diagnosed (mPAP < 25 mmHg). The results of this study demonstrated the efficacy of integrating DL-CFD and eDL-CFD for non-invasive diagnosis of PH. The deep learning model's predictions closely matched the simulation results, showcasing high accuracy and reliability. Comparative analysis revealed that while the correlation between RHC and the developed CFD and DL-CFD methods was lower than traditional echocardiography, eDL-CFD method exhibited a higher correlation with RHC and improved diagnostic accuracy. The area under the curve (AUC) for the combined method was 98.9%, significantly higher than the 94.6% for echocardiography alone. Stratified analysis highlighted that the combined approach improved specificity to 94.1% from 76.4%, maintaining a high sensitivity of 97.3%. This indicates the potential of the combined method to serve as a more reliable non-invasive diagnostic tool for pulmonary hypertension.

These results indicate that the eDL-CFD approach can be a viable non-invasive alternative for diagnosing PH, potentially offering improved diagnostic accuracy and reliability over traditional echocardiography alone. This study demonstrates the potential of eDL-CFD for non-invasive PH diagnosis, supporting personalized treatment planning and accurate prediction of disease progression. Future research will focus on utilizing diverse datasets and applying data augmentation techniques to enhance the model's generalizability and accuracy.

Key words: pulmonary hypertension, hemodynamics, deep learning, computational fluid dynamics, non-invasive diagnosis

Development of Predictive Model based on Medical Image for Prediction of Diagnosis and Treatment Prognosis in Patients with Pulmonary Hypertension

Seongmin Ha

Graduate Program in Biomedical Engineering
The Graduate School, Yonsei University

(Directed by Professor Hyuk-Jae Chang)

I. INTRODUCTION

1. Rare Incurable Condition: Pulmonary Hypertension

Pulmonary hypertension (PH) is when the pressure in the pulmonary arteries is abnormally high. This causes the pulmonary arteries to narrow, or the blood vessel walls in the lungs to thicken, increasing resistance to blood flow. PH places excessive strain on the heart and lungs, and if left untreated, it can gradually worsen and lead to heart failure or other serious health problems. Normal pulmonary artery pressure is less than 25 mmHg, but in patients with PH, this pressure is measured at rest above 25 mmHg **(Figure 1)**[1-3].

PH can be caused by various causes, and the main causes are genetic factors, heart disease, lung disease, and certain drugs or toxins. PH is broadly classified into five types according to the cause, and each type has different pathological characteristics and treatment methods. For example, primary pulmonary hypertension (pulmonary arterial hypertension, PAH) often has an unknown cause, and secondary pulmonary hypertension is caused by another disease of the heart or lungs[4, 5]. The prognosis and survival rate of

PH vary depending on the stage and treatment method at the time of diagnosis, and the prognosis is better if it is detected early and treated appropriately. **(Table 1)** [6-8].

A variety of testing methods are needed to diagnose pulmonary hypertension. The initial diagnosis is performed through noninvasive echocardiography, which estimates whether pulmonary artery pressure is elevated. However, echocardiographic estimates can sometimes be inaccurate compared to invasive right heart catheterization (RHC). RHC is considered the gold standard for diagnosing PH and directly measures pulmonary artery pressure (PAP). This discrepancy can lead to delayed diagnosis or unnecessary right heart catheterization. In addition, tests such as blood tests, computed tomography (CT), and magnetic resonance imaging (MRI) can be performed to determine the cause.

PH is a disease that occurs worldwide, and the prevalence and incidence vary by region and population group. While the prevalence is relatively low in North America and Europe, the prevalence is high in Africa and some parts of Asia. These differences are mainly due to genetic factors, environmental factors, and differences in access to medical care. As awareness of PH increases worldwide, diagnostic and treatment methods steadily improve. However, there are still many challenges, such as difficulty in early diagnosis and high treatment costs[9-12].

PH often has delayed diagnosis because symptoms are not clear in the early stages. Noninvasive echocardiography is useful for initial screening, but its accuracy may be limited due to discrepancies with invasive right heart catheterization. Therefore, the development of faster and more accurate diagnostic methods is needed. New noninvasive and cost-effective diagnostic technologies can enable early detection and treatment of pulmonary hypertension, thereby improving patients' quality of life[13, 14].

Table 1. Clinical classification of pulmonary hypertension

Group	Type
1	Pulmonary arterial hypertension
2	Pulmonary hypertension with left-heart disease
3	Pulmonary hypertension associated with lung disorders, hypoxemia, or both
4	Pulmonary hypertension due to pulmonary artery obstructions
5	Miscellaneous (unclear or multifactorial mechanisms)

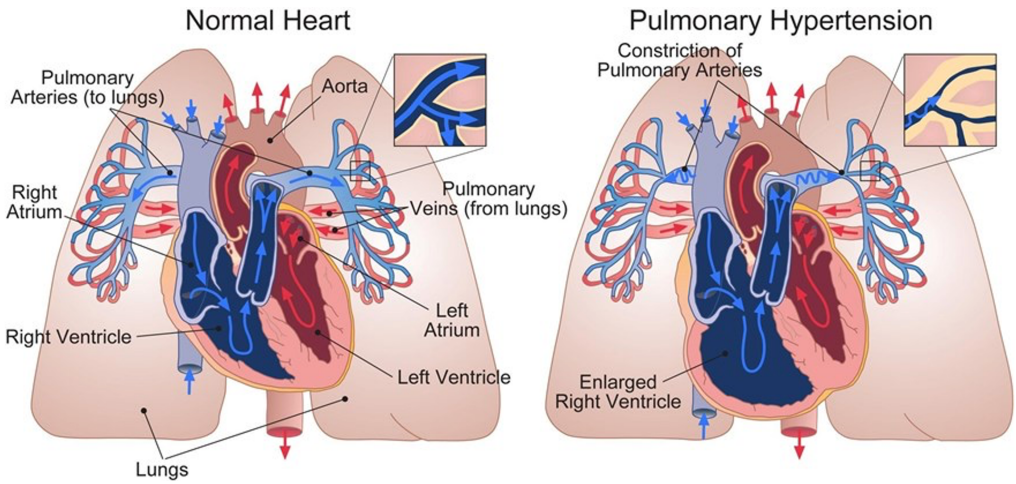

(a) (b)

Figure 1. Pulmonary hypertension, (a): Normal pulmonary artery pressure is 8~25 mmHg at rest, (b): Pulmonary hypertension is pressure in the pulmonary artery that is greater than 25 mmHg at rest or 30 mmHg during physical activity.

2. Diagnostic Modalities for PH

PH is a severe and progressive disorder characterized by elevated PAP and vascular resistance, leading to right heart failure and reduced exercise capacity. The diagnostic process for PH is multifaceted, involving various modalities to assess and manage the condition accurately[1, 3].

Initial clinical suspicion of PH arises from symptom observation and physical examination. However, definitive diagnosis requires hemodynamic assessment primarily through RHC. RHC is considered the gold standard for diagnosing PH, as it directly measures mPAP, PAWP, and cardiac output, providing essential data for confirming PH and differentiating it from other forms of pulmonary hypertension[5, 15].

Transthoracic echocardiography (TTE) plays a pivotal role in the initial screening and evaluation of suspected PH cases. TTE, a non-invasive imaging modality, estimates pulmonary artery pressures by measuring tricuspid regurgitant velocity. It also assesses the right ventricle's size, function, and pressure overload. Despite its utility, TTE alone cannot definitively diagnose PH but serves as an invaluable tool in early identification and risk stratification of patients. Currently, TTE is widely used for the primary diagnosis of pulmonary hypertension, but it is less accurate compared to RHC. This discrepancy can lead to unnecessary RHC procedures for some patients, while missing those who need it, thereby delaying the diagnosis[16, 17].

Computed Tomography (CT) supplements TTE by providing detailed structural information about the thoracic cavity. CT scans are instrumental in identifying and characterizing lung parenchymal disease, assessing pulmonary vasculature, and evaluating for thromboembolic disease **(Figure 2)**. Moreover, CT imaging offers insights into the differential diagnosis of PH, assisting in identifying underlying causes and contributing to prognostic assessments[18-20].

Other diagnostic tests, such as pulmonary function tests, blood tests for biomarkers, and exercise testing, contribute to the comprehensive evaluation of PH. These tests provide information about the functional status of patients, disease severity, and response to therapy,

thereby guiding treatment decisions[4, 5, 21].

The diagnosis of PH is complex and requires a combination of clinical evaluation and multiple diagnostic modalities. RHC remains the definitive method for diagnosis, while non-invasive techniques like TTE and CT scans play crucial roles in the initial evaluation, risk stratification, and ongoing management of PH patients. Given the fatal nature of PH, even missing a single diagnosis can delay early treatment, leading to poor outcomes. Therefore, there is a need for a superior non-invasive approach to diagnose PH that surpasses the current echocardiographic methods, using RHC as the reference standard[13, 22].

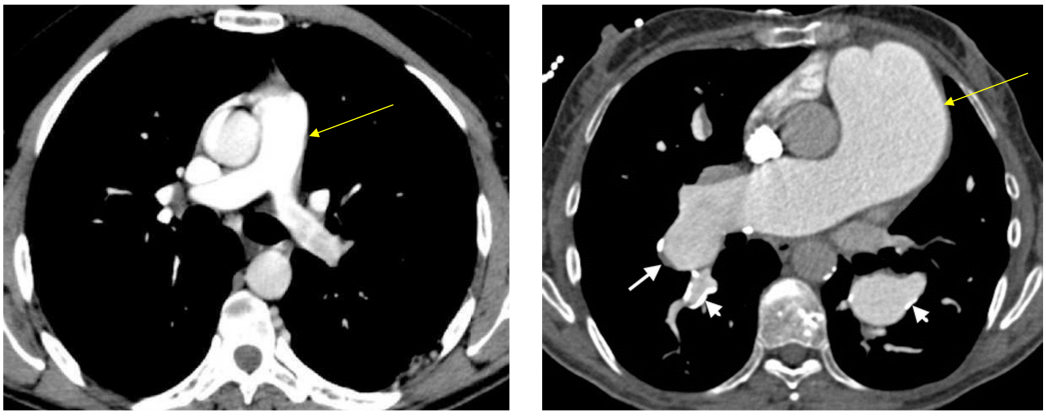

Figure 2. Normal pulmonary artery CT image of a healthy individual (left) and an enlarged pulmonary artery CT image of a patient with PH (right).

3. Hemodynamic Analysis in PH

PH is a complex cardiovascular condition characterized by increased pressure in the pulmonary arteries. Traditional diagnostic methods have relied heavily on invasive procedures like right heart catheterization. However, recent advancements in non-invasive diagnostic technologies, notably computational fluid dynamics (CFD), have opened new avenues for assessing and managing PH[4, 23].

CFD is a branch of fluid mechanics that uses numerical analysis and algorithms to solve and analyze problems involving fluid flows. In the context of PH, CFD utilizes advanced computational algorithms, such as the finite difference method (FDM), finite element method (FEM), and finite volume method (FVM), to solve the Navier-Stokes equations, which describe the motion of viscous fluid substances. This approach allows for the detailed visualization and analysis of blood flow dynamics within the pulmonary vasculature[24, 25].

The application of CFD in PH provides invaluable insights into hemodynamic parameters, which are crucial for understanding the progression and severity of the disease. Simulations using patient-specific 3D models enable clinicians to visualize blood flow patterns, assess flow velocity, and evaluate parameters such as wall shear stress (WSS). WSS is particularly significant as it indicates the mechanical stress exerted on the vascular endothelium, a critical factor in the pathophysiology of PH[26, 27].

One of the significant advantages of CFD in PH diagnosis is its ability to provide superior spatial and temporal resolutions of blood flow. Unlike traditional imaging modalities, CFD simulations can resolve complex pathological hemodynamic challenges, offering detailed insights into the disturbed flow patterns typical in PH patients. This level of detail can be critical in diagnosing challenging cases where conventional methods may not provide sufficient information[28, 29].

Furthermore, CFD simulations can potentially enhance personalized medicine approaches in PH. Using patient-specific models, clinicians can predict disease progression, assess the efficacy of therapeutic interventions, and tailor treatment plans to individual

patient needs. This precision approach could lead to better outcomes and improved quality of life for PH patients[30].

CFD represents a revolutionary step forward in the non-invasive diagnosis of PH. Its ability to provide detailed insights into blood flow dynamics and its application in patient-specific models offers significant advantages over traditional diagnostic methods. As CFD technology continues to evolve, it promises to further enhance our understanding and management of PH **(Figure 3)** [31, 32].

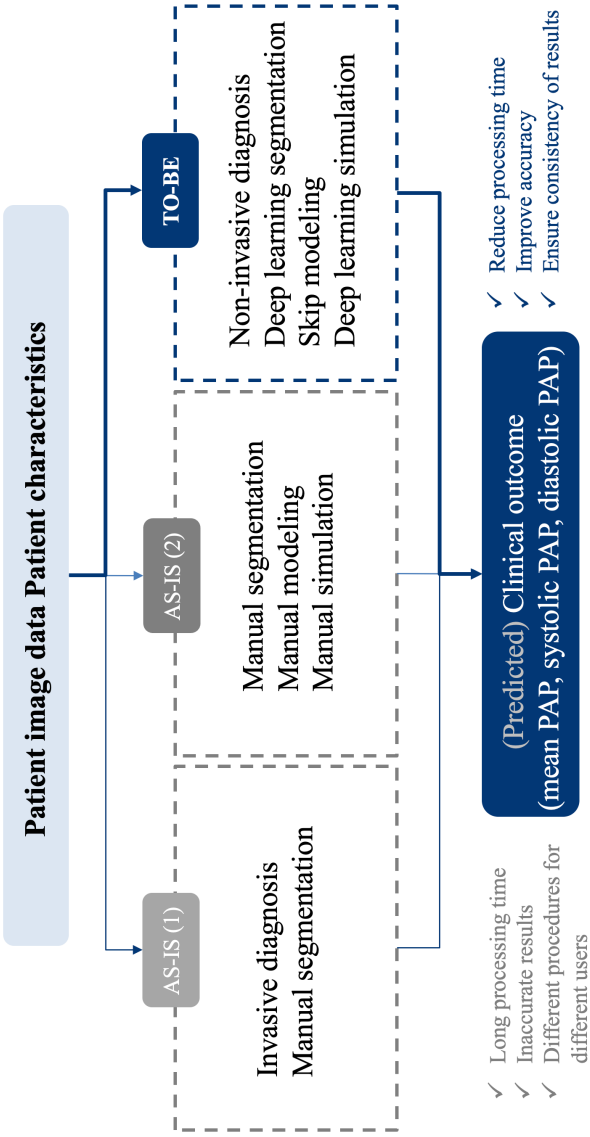

Figure 3. The AS-IS (1) process for clinical diagnosis involves invasive tests with significant operator involvement and structural examination. The AS-IS (2) utilizes non-invasive methods but requires operator intervention and longer processing times. The TO-BE process aims to achieve rapid clinical outcomes using non-invasive methods while minimizing operator involvement.

4. Deep Learning with CFD Simulation for PH Diagnosis

The advent of deep learning in the medical and healthcare sector marks a transformative era, offering rapid and accurate diagnostics across various fields, including cardiology. Recently, deep learning technologies have been successfully implemented in the medical field, especially in diagnosing cardiac diseases. These technologies have shown exceptional capability in performing repetitive image analysis tasks comparable to professional medical practitioners[33-37].

Particularly in the context of pulmonary hypertension, a condition where diagnosis crucially depends on changes in blood flow and pressure, the use of non-invasive imaging techniques like CT and magnetic resonance imaging (MRI) has been paramount. However, these methods often involve time-consuming processes like segmentation and localization, with the accuracy heavily dependent on the analyst's expertise. Deep learning transforms the field by offering rapid and precise analysis, enhancing patient care through timely and accurate diagnostics[38, 39].

Our study utilizes non-invasive imaging tests, specifically echocardiography and CT, in conjunction with deep learning with CFD simulations (DL-CFD) and echocardiography + DL-CFD (eDL-CFD) supplemented with analytical values calculated using Mahan's equation from echocardiography. This approach is compared against the current gold standard, RHC, which is an invasive diagnostic procedure. The goal is to validate the significance of the developed technology compared to RHC and to ascertain its accuracy in distinguishing between regular patients and those suffering from PH[40].

Deep learning in medical imaging and CFD simulation represents a significant step forward in PH diagnosis. By leveraging advanced algorithms and large datasets, deep learning models can efficiently process and analyze complex medical images. This capability is particularly advantageous in CFD simulations, where the accurate representation and analysis of blood flow dynamics are crucial. In PH, where subtle changes in pulmonary hemodynamics are pivotal, DL-CFD and eDL-CFD can provide

more detailed and accurate assessments than traditional methods[33, 41-44].

Physics-informed neural networks (PINNs) are another innovative approach that integrates physical laws into neural network training, enhancing the model's accuracy and generalizability. PINNs use governing equations of physics, such as Navier-Stokes for fluid dynamics, as constraints during the training process, allowing them to learn from both data and physical principles. This integration is particularly beneficial in medical applications like CFD simulations, where accurate modeling of hemodynamic conditions is essential. Representative works in this area include Raissi et al.'s seminal papers on physics-informed deep learning[45-47].

Furthermore, deep learning algorithms can continuously learn and improve from new data, potentially increasing diagnostic accuracy. This aspect mainly benefits handling diverse patient populations and complex clinical scenarios, enabling personalized and precise healthcare delivery[34-36, 48, 49].

In conclusion, incorporating deep learning in non-invasive diagnostic methods, particularly in the context of PH, presents a promising frontier in medical technology. By combining, this approach aims to enhance the accuracy and efficiency of PH diagnostics, potentially surpassing the capabilities of traditional methods and paving the way for more patient-centric and non-invasive diagnostic procedures **(Figure 4)**[35].

This research aims to evaluate the efficacy of a combined model incorporating noninvasive tests such as echocardiography, CT, CFD, and deep learning, using RHC as the gold standard. Furthermore, the study seeks to determine the potential of this combined approach as an alternative or complementary method to the widely used echocardiography for diagnosing PH.

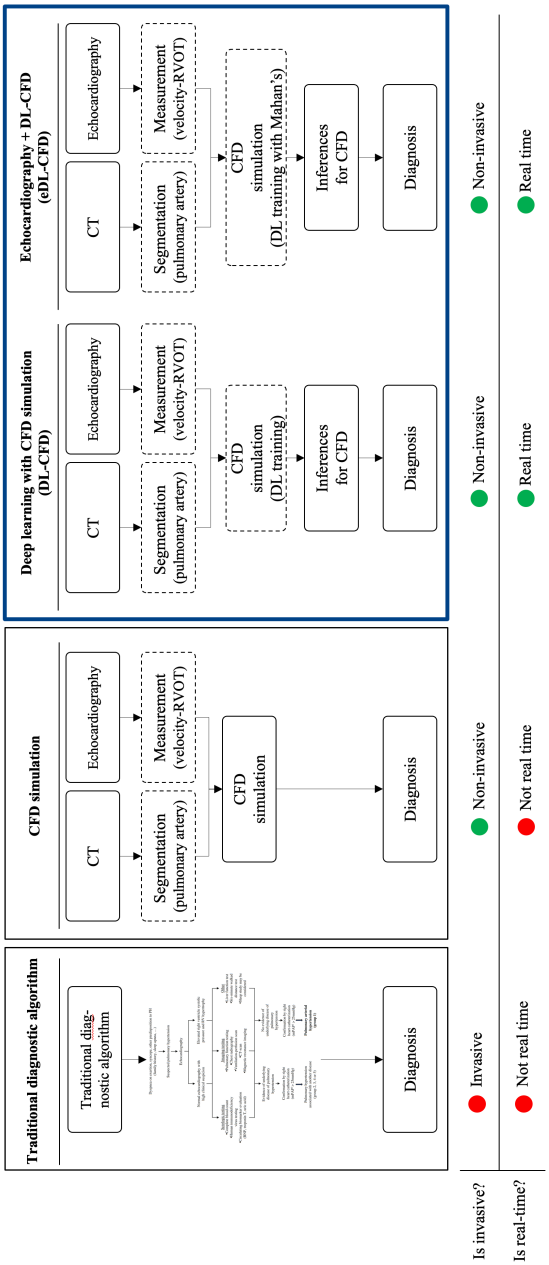

Figure 4. Traditional diagnosis of PH involves invasive methods and is not real-time. Using CFD simulation provides a non-invasive method, but it is also not real-time. Applying DL-CFD and eDL-CFD enables real-time, non-invasive diagnosis.

II. MATERIALS and METHODS

1. Subjects

Between 2008 and 2019, a retrospective cohort was composed of 92 patients who underwent RHC for various clinical reasons, including PAH or other conditions causing PH. This cohort included 75 patients diagnosed with PH (mPAP > 25 mmHg) and 17 patients who were suspected of having PH and underwent RHC but were not diagnosed with PH (mPAP < 25 mmHg). Additionally, all patients underwent echocardiography and computed tomography (CT). Participants were selected using random sampling to ensure a representative sample of the patient population. This study received approval from the IRB of Severance Hospital. Before enrollment, informed consent was obtained in writing from all participants. This cohort allowed for a comprehensive analysis of diagnostic modalities and their effectiveness in assessing and managing PH, contributing valuable insights into these patients' clinical characteristics and outcomes.

2. Right Heart Catheterization

All patients diagnosed with PH underwent RHC using a balloon-tipped, 7-Fr SwanGanz CCombo PA catheter (Baxter, Irvine, CA, USA), which was inserted either via the right or left femoral vein. During the catheterization procedure, patients were positioned supine, resting comfortably while breathing room air, ensuring they were stable. Hemodynamic data were collected while the patients were at rest to obtain accurate and consistent measurements. The following hemodynamic parameters were meticulously measured: systolic pulmonary artery pressure (sPAP), diastolic pulmonary artery pressure (dPAP), mPAP, right atrial pressure (RAP), PAWP, cardiac output (CO) using thermodilution, and cardiac index (CI), which is the CO normalized to body surface area. PVR was calculated using the values of mPAP, PAWP, and CO, providing a comprehensive assessment of the pulmonary circulatory system. stroke volume (SV) was also calculated during RHC using the measured CO and heart rate. These detailed hemodynamic assessments through RHC were critical in accurately diagnosing and evaluating the severity of PH in these patients, facilitating the appropriate clinical management and therapeutic decision-making process.

3. Velocity Segmentation in Echocardiography

Echocardiography represents a cornerstone in the non-invasive PH diagnosis, offering a convenient and widely accessible method to assess hemodynamic variables. TTE images were utilized for this study, with inclusion criteria mandating that all echocardiographic footage conformed to standard views and visual norms. Exclusion criteria were set to omit patients diagnosed with conditions that could confound the interpretation of echocardiographic data, such as heart failure, coronary artery disease, valvular heart disease, or pregnancy, and those with substandard image quality obtained from non-standardized scans.

Measurements were explicitly focused on cases where at least one view in the Doppler echocardiogram allowed for calculating mPAP. Three primary methods, utilizing spectral Doppler, were employed to measure pulmonary artery pressure:

A. Average Pulmonary Artery Pressure Using Tricuspid Regurgitation (Based on Systolic Pulmonary Artery Pressure)

This method involved the use of pulmonic valve (PV) pulse wave (PW) Doppler, targeting the right ventricular outflow tract (RVOT) to determine the PV PW. This approach is instrumental in calculating the mPAP, with the RVOT velocity maximum measured and applied in a specific formula for mPAP calculation. Furthermore, the mPAP can be estimated from the sPAP using empirical relations.

$$sPAP = 4 \times (TRV)^2 + RAP,$$
$$mPAP = 4 \times \left(RVOT_{velocity\ max}\right)^2 + RAP.$$

B. Mahan's Method for Systolic Flow Acceleration Time in the Right Ventricular Outflow Tract

Using Mahan's equation, this method entailed measuring pulmonic valve continuous wave (PV CW) Doppler, targeting pulmonic regurgitation (PR) to derive measurements. The PR velocity maximum was measured and then applied in another specific formula to calculate the mPAP.

$$PAP = \frac{constant}{Acceleration\ time} + adj.$$

C. Diastolic Pulmonary Artery Regurgitation Velocity Measurement

The measurement was taken by targeting tricuspid regurgitation (TR) at the tricuspid valve and measuring the TR continuous wave (TV CW). The TR velocity maximum was then used in a formula to calculate the mPAP **(Figure 5)**.

$$mPAP = 4 \times (DPRV)^2 + DRAP.$$

Combined with the image acquisition and interpretation standardization, these methodologies provide a comprehensive and reliable approach to the echocardiographic assessment of PH. Multiple Doppler techniques enhance diagnostic accuracy, allowing for a detailed evaluation of the hemodynamic status in patients with suspected or confirmed PH. The application of these methods aligns with current best practices in echocardiographic diagnostics and underscores the role of non-invasive imaging in managing pulmonary hypertension.

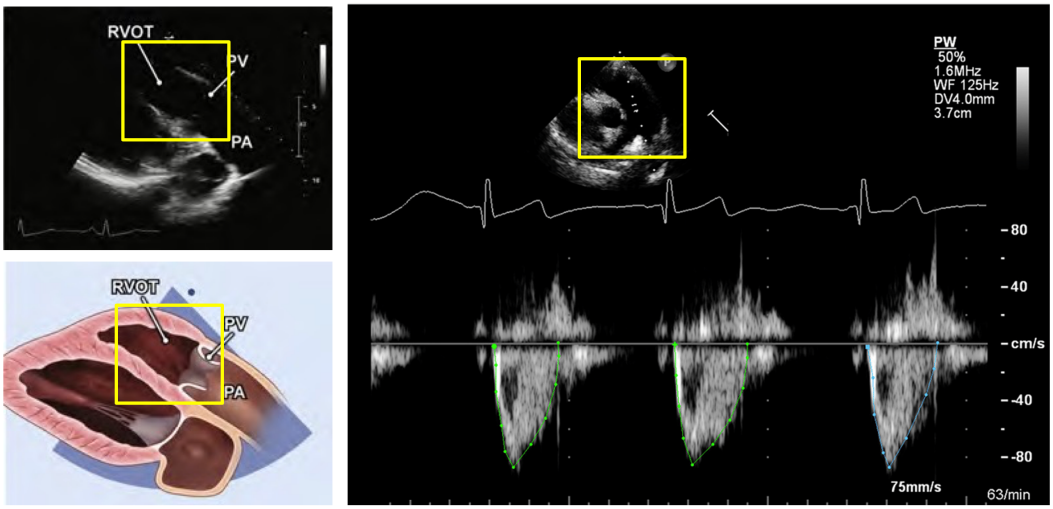

Figure 5. Confirmation of the RVOT location in B-mode using echocardiography, followed by spectral Doppler imaging to measure blood flow velocity at the RVOT

D. Spectral Doppler Segmentation

The segmentation of Doppler signals from echocardiography data is a critical step in our methodology, particularly for accurately capturing the velocity profiles necessary for subsequent CFD simulations. This process begins with the selection and preprocessing of RVOT spectral Doppler images stored in digital imaging and communications in medicine (DICOM) format. The selected Doppler images are converted into a standardized format suitable for annotation, ensuring they meet the quality criteria necessary for creating training datasets. Using a commercial framework, 2D masks are generated for each Doppler image to delineate the Doppler signal regions within the RVOT. These annotations, performed by trained experts, ensure high accuracy and create a reliable ground truth dataset for model training.

The annotated Doppler images serve as the foundation for training a segmentation model based on the U-net architecture, which is well-suited for biomedical image segmentation. The U-net model, with its encoder-decoder structure and skip connections, captures fine details in complex medical images. The encoder compresses the input image

to capture essential features, while the decoder reconstructs the image to its original dimensions, providing a detailed segmentation map. The skip connections enhance the segmentation accuracy by retaining spatial information. The annotated dataset is split into training and validation sets, and the U-net model is trained using these datasets. Data augmentation techniques such as rotation, scaling, and translation are employed to enhance the model's robustness. The Adam optimizer is used to optimize the model parameters, with cross-entropy as the loss function to handle the segmentation task effectively **(Figure 6)**. The model's performance is evaluated using metrics such as the dice similarity coefficient (DSC), which measures the overlap between the predicted segmentation and the ground truth.

Once trained, the U-net model is employed to segment RVOT spectral Doppler signals from new echocardiography data, significantly reducing the manual effort and time required for Doppler signal extraction. The trained model processes new RVOT Doppler images, generating segmentation masks that accurately delineate the Doppler signals. These masks are reviewed for consistency and accuracy, ensuring that the segmented regions correspond precisely to the actual Doppler signals. The segmented Doppler signals are then converted into velocity profiles, which serve as inlet boundary conditions for CFD simulations. The velocity profiles are extracted by averaging the Doppler signal intensities over time, providing a detailed representation of the blood flow dynamics through the RVOT. These extracted inlet velocity profiles are integrated into the CFD simulation framework, enabling accurate modeling of blood flow through the pulmonary arteries. This integration ensures that the simulations reflect realistic hemodynamic conditions, enhancing the validity of the study's findings.

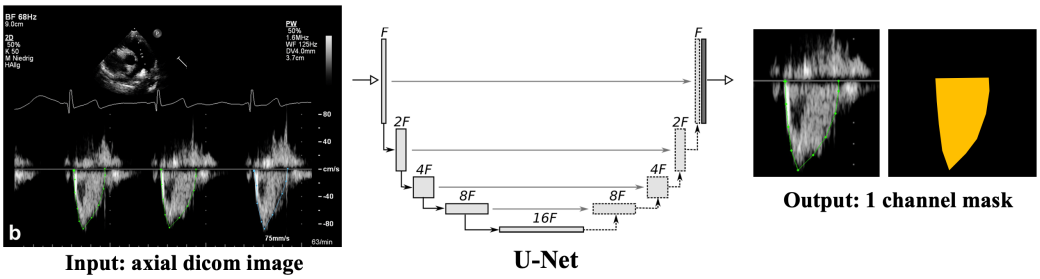

Figure 6. Using echocardiography to capture spectral Doppler images at the RVOT and annotating the blood flow velocity profile data to train a U-net based segmentation model.

4. Segmentation of the Pulmonary Artery in Computed Tomography

The CT scans utilized in this study were acquired between 2008 and 2019. Of the 92 CT scans, 51 were performed using Siemens, 23 using GE, 15 using Philips, and 3 using Canon. The scans were obtained with tube voltages of 140kVp (n=32), 120kVp (n=3), and 100kVp (n=57). The slice thicknesses were 1.25mm (n=17), 1mm (n=72), and 0.625mm (n=3). All CT scans were acquired with prospective electrocardiogram (ECG) gating while administering contrast agents.

Deep learning-based segmentation was performed to extract the three-dimensional structure of the pulmonary artery automatically. First, to create ground truth data, 2-dimensional masks for each CT slice were generated using the commercial framework, 3-matics (Materialise NV, Leuven, Belgium). The range for mask generation was set from the main pulmonary artery to the right/left pulmonary artery, excluding branches from the first branch onwards. The DICOM image size was 512x512, and the z-slice range was approximately 200 to 400.

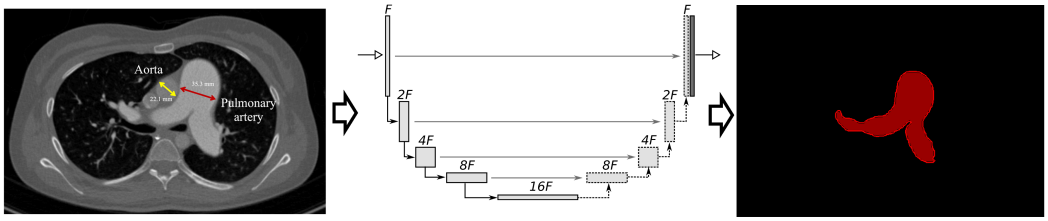

Figure 7. After performing contrast-enhanced CT imaging of the pulmonary artery, the data is masked and annotated to train a U-net based segmentation model.

The network architecture comprised an encoder and decoder connected by skip connections. In the encoder, the image size was reduced through 2D convolutional layers, batch normalization, and ReLU activation, with feature extraction co-occurring. The

subsequent application of max pooling reduced the size of the feature map, leading to the loss of local information. Conversely, the decoder also involved 2D convolutional layers, batch normalization, and ReLU activation, but using upsampling layers resulted in the reflection of feature information onto the image. Finally, the network was configured for mask inference by concatenating dimensions and applying a softmax function after the skip connections, utilized at each layer stage to preserve essential feature information and prevent the loss of critical features. The loss function employed was cross-entropy, which is defined as:

$$L(y, \hat{y}) = -\sum_i y_i \log(\hat{y}_i),$$

Where y represents the actual label, and $\hat{y}$ is the predicted probability **(Figure 7)**.

To evaluate the performance of the segmentation, the DSC was used to assess the congruence between the ground truth data and the resulting segmentation masks.

$$DSC = \frac{2 \times TP}{(TP + FP) + (TP + FN)}$$

5. Model geometric parameters modification

To perform accurate CFD simulations, it is essential to ensure that the geometric models of the pulmonary artery are precise and representative of the actual patient-specific anatomy. The modifications to the geometric parameters of the models are performed as follows:

A. Preprocessing and Mesh Generation

The initial step involves preprocessing the segmented pulmonary artery structures obtained from CT scans. The raw segmented data are smoothed to remove noise and improve the quality of the geometric model. Smoothing algorithms, such as Gaussian smoothing or Laplacian smoothing, are applied to achieve a balance between retaining anatomical details and eliminating artifacts.

Once the smoothing process is completed, the geometric model is converted into a mesh suitable for CFD simulations. This involves generating a high-quality, computationally efficient mesh that accurately represents the pulmonary artery's 3D structure **(Figure 8)**. The meshing process typically includes:

Surface meshing: Creating a fine mesh on the surface of the pulmonary artery using triangular or quadrilateral elements.

Volume meshing: Filling the interior of the pulmonary artery with tetrahedral or hexahedral elements to create a volumetric mesh suitable for flow simulations.

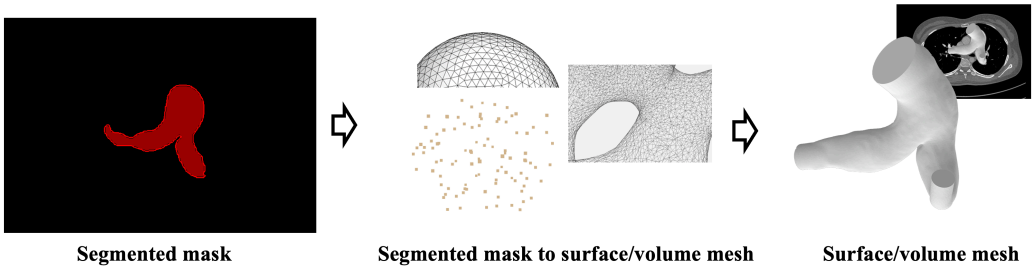

Figure 8. Extracting 3D pulmonary artery masks from CT images, followed by preprocessing such as 3D smoothing, and generating a surface mesh.

B. Boundary Conditions Definition

To ensure realistic simulation results, appropriate boundary conditions are defined for the CFD model. This includes specifying the inlet and outlet boundaries, wall boundaries, and any internal boundaries within the pulmonary artery **(Figure 9)**:

Inlet boundary: The main pulmonary artery serves as the inlet where blood flow enters. Flow velocity or pressure profiles are applied based on physiological data.

Outlet boundaries: The right and left pulmonary arteries act as outlets. Outlet pressure or flow distributions are assigned to simulate realistic blood flow exiting the model.

Wall boundaries: The arterial walls are treated as no-slip boundaries, meaning that the fluid velocity at the wall surface is zero, simulating the interaction between the blood and the vessel wall.

C. Geometric Parameter Adjustments

Modifications to geometric parameters may be necessary to represent patient-specific conditions accurately. Adjustments include scaling the model to match patient dimensions, refining regions with complex flow dynamics, and incorporating anatomical variations such as bifurcations or stenosis.

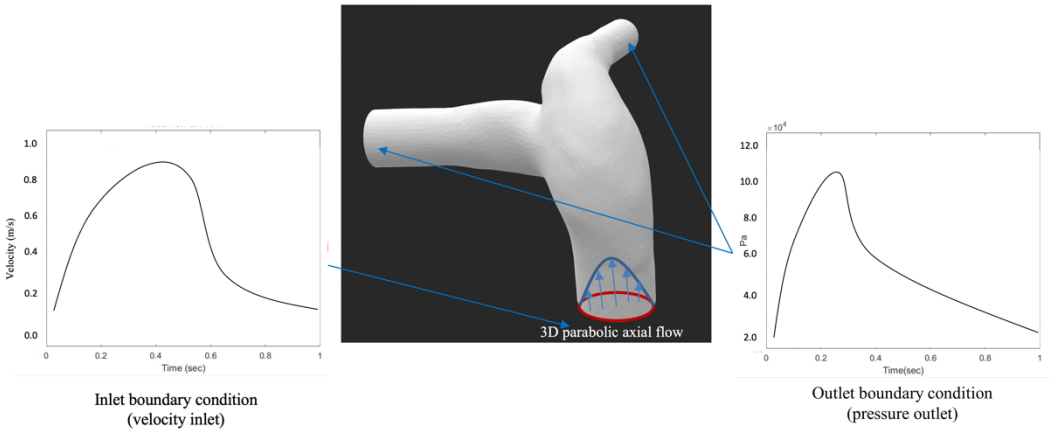

Figure 9. Using spectral Doppler to input inlet information of the 3D pulmonary artery geometry and employing RHC wedge pressure for outlet information in the CFD simulation.

6. Simulated operation of CFD

The CFD simulation setup for this study involved a comprehensive definition of physical and numerical parameters governing the fluid dynamics of blood flow within the pulmonary artery. The Navier-Stokes equations, which describe the motion of viscous fluid substances, were solved numerically to ensure mass conservation and account for the forces acting on the fluid, including pressure and viscous forces.

Blood was modeled as an incompressible, non-Newtonian fluid with properties defined by the Carreau model to capture its shear-thinning behavior. The fluid properties were set with a density of 1060 kg/m³, and the dynamic viscosity was determined by the equation:

$$\mu = \mu_\infty + (\mu_0 - \mu_\infty)[1 + (\lambda\gamma)^2]^{\frac{n-1}{2}}$$

Where $\lambda = 3.313\ s,\ n = 0.3568,\ \mu_0 = 0.056\ kg/ms,\ \mu_\infty = 0.0035\ kg/ms.$

Boundary conditions were critical for the accuracy of the CFD model. The inlet condition was defined at the RVOT using a mass flow inlet boundary, specifying the rate of blood entering the pulmonary artery. The outlet boundary condition was based on the PAWP measured during RHC. Wall boundaries were treated with a no-slip condition, ensuring the fluid velocity at the arterial wall surface was zero.

A transient solver was used to capture the dynamic behavior of blood flow over time, implementing the k-epsilon turbulence model to account for turbulence effects. The pressure-based solver was chosen for its ability to resolve pressure and velocity fields accurately. The simulation ran over an R-R interval of 1 second, sampled at 60 points to capture temporal variations in hemodynamic parameters.

The FVM was employed to discretize the governing equations, with time-stepping schemes designed to handle the transient nature of the simulations. Convergence criteria were set to monitor residuals for continuity, momentum, and other relevant variables, ensuring accurate and stable results when residuals dropped below 10^{-6}.

Post-processing involved extracting meaningful hemodynamic parameters such as velocity fields, pressure distribution. These parameters provided insights into the flow dynamics within the pulmonary artery, highlighting regions of high velocity, analyzing pressure gradients, and assessing the mechanical stress exerted on the vascular endothelium. Results were extracted at 60 time points throughout the cardiac cycle, offering a detailed temporal analysis of hemodynamic changes **(Figure 10)**.

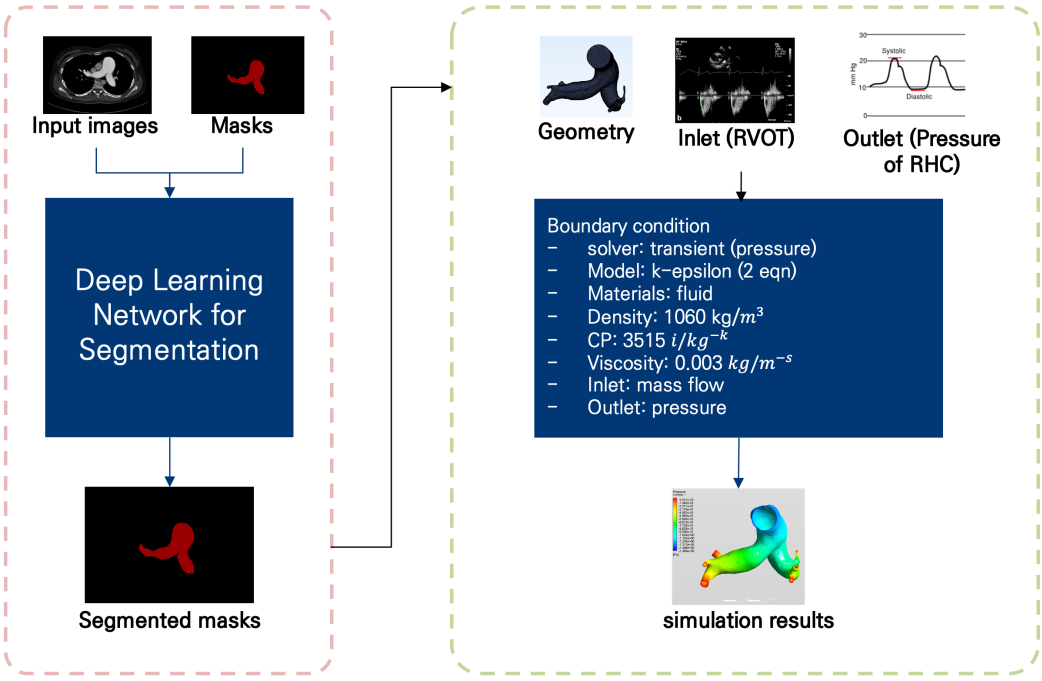

Figure 10. Generating a surface mesh from the segmentation results of CT geometry using deep learning and inputting the RVOT velocity from spectral Doppler and wedge pressure from RHC into a CFD simulation to derive pressure-inclusive volume information.

7. Patient specific deep learning with CFD simulation

To enhance the diagnostic process, patient-specific DL-CFD and eDL-CFD were developed. The initial step involved the segmentation of pulmonary artery geometries from CT scans, which were then converted into surface meshes, capturing detailed contours and structural features. The corresponding volume mesh was generated using the surface mesh as a reference, ensuring accurate volumetric representation of the pulmonary artery. These meshes were annotated with hemodynamic data such as mPAP values **(Figure 11)**.

The geometric PointNet framework was utilized to model the hemodynamic behavior within the pulmonary artery. PointNet, designed to handle 3D point cloud data, was suitable for analyzing the surface and volume meshes. The model employed a dual-layer feature extraction process: local features were extracted from both the surface and volume meshes, capturing details such as curvature, area, and centroid pressure values. Skip connections were integrated to preserve essential information and enhance learning.

Incorporating patient-specific meta-features such as age and gender, the model processed these inputs through dedicated layers to extract weights, which were then concatenated with geometric features. The combined weights from both the local feature layers and the meta-feature layers were further processed to extract global features, encapsulating the patient's overall condition. This approach ensured a comprehensive analysis of both structural and functional aspects of the pulmonary artery **(Figure 12, 13).**

Additionally, a model was developed that included the results of the Mahan equation analyzed from echocardiography as part of the meta-features in the deep learning model (eDL-CFD). This model was designed to facilitate mutual complementation between hemodynamic information (CFD) and conventional examination methods (echocardiography, CT). **(Figure 12, 13)**.

The final layer of the model predicted the mPAP by leveraging the comprehensive feature set. The training process involved minimizing the mean absolute error (L1 loss function) between predicted and actual mPAP values, defined as:

$$\arg\min L(\theta) = \frac{1}{n}\sum_{i=1}^{n}\left|Y_i - \widehat{Y_i}\right|$$

where Y_i represents the actual mPAP and $\widehat{Y_i}$ denotes the predicted mPAP. The Adam optimizer was used for efficient convergence during training.

Performance was evaluated using mean absolute error (MAE) and root mean square error (RMSE), with RMSE defined as:

$$RMSE = \sqrt{\frac{1}{N}\sum_{\theta=1}^{N_y}\sum_{s=1}^{N_x}||(R(s,\theta) - \tilde{R}(s,\theta)||^2}.$$

where $R(s,\theta)$ and $\tilde{R}(s,\theta)$ represent the actual and predicted values, respectively.

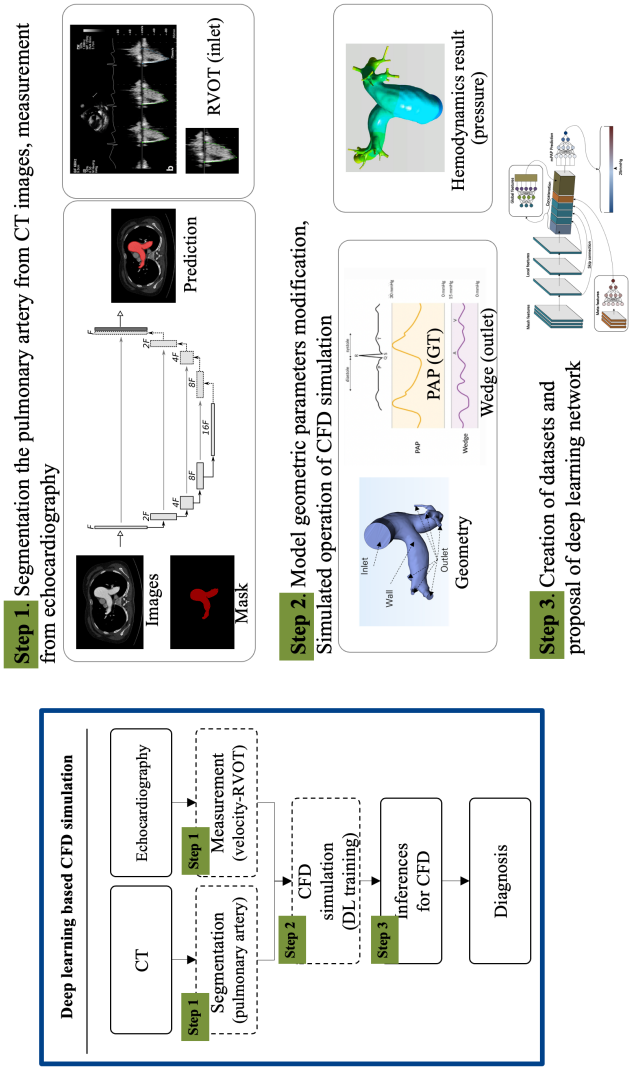

Figure 11. The DL-CFD and eDL-CFD consists of three steps. Step 1: Using deep learning to extract geometry from CT and velocity profile at RVOT from echocardiography. Step 2: Using the extracted geometry and velocity profile (inlet) and wedge pressure from RHC (outlet) to perform hemodynamic calculations. Step 3: Using the calculated hemodynamics (volume mesh) along with the existing surface mesh and meta-data (e.g., age, gender, Mahan's results) to train a PointNet for predicting PAP.

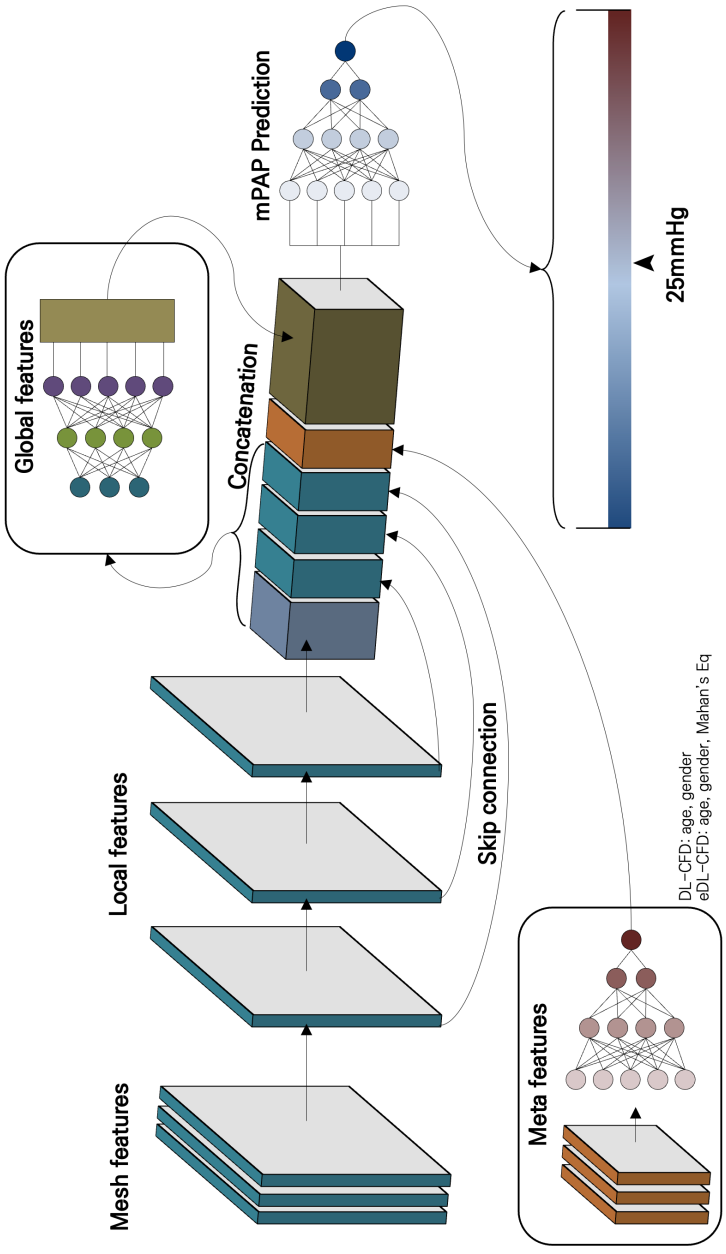

Figure 12. Inputting surface mesh and volume mesh (PAP) data into mesh features layer and concatenating with meta-data (e.g., age, gender, Mahan's results) and a layer for extracting global state information to ultimately predict mPAP.

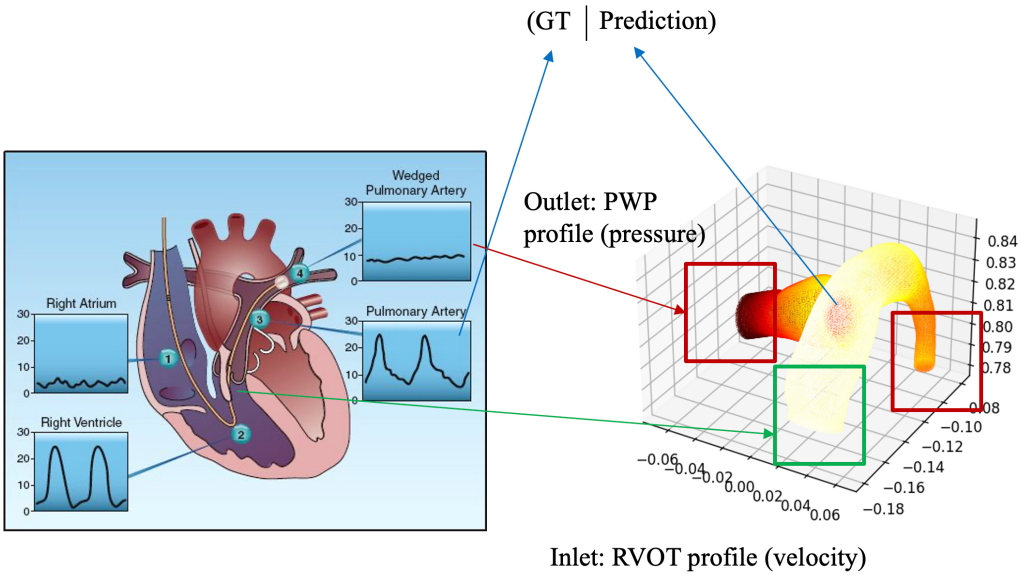

Figure 13. Matching the predicted results with anatomical locations at inlet/outlet.

8. Statistics

Demographic and clinical characteristics were summarized using mean values and standard deviations for continuous variables and frequencies and percentages for categorical variables. Bivariate comparisons between measured and predicted results were assessed using paired t-tests and Pearson correlation coefficients. A p-value of less than 0.05 was considered statistically significant. Bland-Altman plots with 95% confidence intervals were calculated for assessing the correlation. Inter-observer and intra-observer reliability were evaluated by the intraclass correlation coefficient (ICC) based on the absolute agreement of single measurements between two observers. The diagnostic performance of each modality for PH was analyzed using area under the curve (AUC) to assess changes in specificity and sensitivity based on a threshold of 25 mmHg. Evaluation metrics including sensitivity, specificity, positive predictive value (PPV), negative predictive value (NPV) and accuracy were also used to assess the method's performance. A p-value less than 0.05 was considered statistically significant. Data analyses were performed using MedCalc statistical software, version 18.2.1 (MedCalc Software bvba, Ostend, Belgium).

III. EXPERIMENTS

1. Patient Characteristics

A total of 92 patients were included in this study, comprising 75 patients diagnosed with PH and 17 patients without PH. The demographic and clinical characteristics of the study population are summarized in Table 1. The PH group had a mean age of 55.3 years (± 16.9), while the non-PH group had a mean age of 59.0 years (± 15.4), with a statistically significant difference ($p < 0.001$). The proportion of females was slightly higher in the PH group (65.3%) compared to the non-PH group (70.5%), also statistically significant ($p < 0.001$). Hemodynamic measurements showed that the PH group had significantly higher dPAP, sPAP, and mPAP values compared to the non-PH group (all $p < 0.001$), **(Table 2)**.

2. Pre-processing

The pre-processing phase involved several critical steps to ensure the accuracy and quality of the data used for CFD simulations and deep learning model training. Firstly, the CT scan data were segmented to isolate the pulmonary arteries, from which surface meshes were generated. This surface meshes were further refined to remove noise and enhance geometric accuracy through smoothing algorithms such as Gaussian and Laplacian smoothing. Subsequently, volume meshes were created using the refined surface meshes as a reference, ensuring a detailed volumetric representation suitable for CFD analysis. These meshes were then annotated with hemodynamic data such as mPAP values obtained from RHC.

3. Implementation Details

The CFD simulations were set up using a transient solver to capture the dynamic behavior of blood flow within the pulmonary artery. The simulations utilized the k-epsilon turbulence model to account for turbulent effects. Blood was modeled as an incompressible, non-Newtonian fluid, with properties defined as density 1060 kg/m^3, specific heat capacity

3515 J/kg·K, and viscosity following the Carreau model. Boundary conditions were specified with mass flow inlet at the RVOT and pressure outlet corresponding to the pulmonary capillary wedge pressure. Each simulation was run over an R-R interval of 1 second, sampled at 60 points to capture temporal variations in hemodynamics.

For the deep learning model, a geometric PointNet was employed. This model was trained using segmented pulmonary artery geometries converted into surface and volume meshes. Local features from these meshes, along with patient-specific meta features (e.g., age, gender), were extracted and concatenated to form a comprehensive feature set. The model was trained to minimize the MAE between predicted and actual mPAP values, using the Adam optimizer for efficient convergence. The model was evaluated using 5-fold cross-validation.

4. Evaluation

The performance of the DL-CFD and eDL-CFD was evaluated using various metrics. The MAE and RMSE were calculated to assess the accuracy of mPAP predictions.

Table 2. Patient Characteristics

	Non-PH	**PH**	***p* value**
Number of subjects	17	75	
Age (years)	59.0 ± 15.4	55.3 ± 16.9	<0.001
Female	12 (70.5%)	49 (65.3%)	<0.001
$dPAP_{RHC}$ (mmHg)	19.5 ± 8.4	32.7 ± 13.7	<0.001
$sPAP_{RHC}$ (mmHg)	43.3 ± 17.2	75.5 ± 23.8	<0.001
$mPAP_{RHC}$ (mmHg)	28.6 ± 9.8	48.8 ± 16.1	<0.001

Values are mean ± standard deviation, or n (%); PAP: pulmonary artery pressure;
RHC: right heart catheterization

IV. RESULTS

The results of this study demonstrated the efficacy of integrating DL-CFD and eDL-CFD for non-invasive diagnosis of PH. The deep learning model's predictions closely matched the simulation results, showcasing high accuracy and reliability. Comparative analysis revealed that while the correlation between RHC and the developed CFD and DL-CFD methods was lower than traditional echocardiography, eDL-CFD method exhibited a higher correlation with RHC and improved diagnostic accuracy. The area under the curve (AUC) for the combined method was 98.9%, significantly higher than the 94.6% for echocardiography alone. Stratified analysis highlighted that the combined approach improved specificity to 94.1% from 76.4%, maintaining a high sensitivity of 97.3%. This indicates the potential of the combined method to serve as a more reliable non-invasive diagnostic tool for pulmonary hypertension.

1. Evaluation Metrics

The segmentation of the pulmonary artery from CT images is a crucial step in the CFD simulation process. In this study, a deep learning-based segmentation model was employed to automatically segment the pulmonary artery from CT scans. The model utilized a U-net architecture, which is well-suited for biomedical image segmentation tasks. The performance of the segmentation model was evaluated using the DSC, which measures the overlap between the predicted segmentation and the ground truth. The DSC value achieved by the model was 85.53, indicating a high level of accuracy in segmenting the pulmonary artery **(Figure 14)**.

The MAE and RMSE were calculated to assess the model's performance. The MAE for PH patients was 2.8 mmHg, and for non-PH patients, it was 3.2 mmHg. The RMSE for PH patients was 3.4 mmHg, while for non-PH patients, it was 3.8 mmHg. These low error values indicate the high precision of the model in predicting hemodynamic parameters.

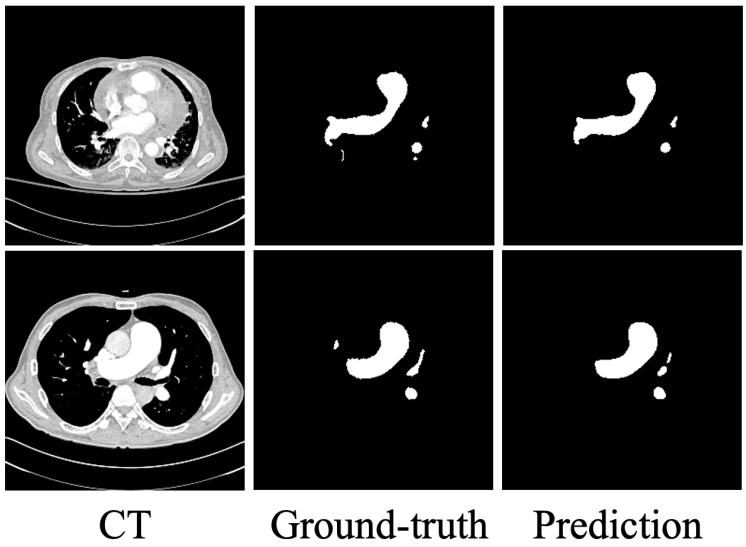

Figure 14. Comparison between the deep learning with segmentation results of the pulmonary artery in CT images and the ground truth.

2. Inter-Observer and Intra-Observer Reliability

The ICC was calculated for inter-observer and intra-observer measurements, showing excellent reliability. The ICC for inter-observer reliability was 0.95, and for intra-observer reliability, it was 0.97, demonstrating high consistency in the model's predictions.

3. Comparative Analysis

A. Comparison of RHC, CFD Simulation and DL-CFD

The deep learning model's performance was compared with traditional diagnostic methods such as RHC and echocardiography. The non-invasive nature of the deep learning model, combined with its high accuracy, presents significant advantages over these traditional methods. RHC, though the gold standard, is invasive and carries risks, whereas the deep learning model offers a safer, non-invasive alternative. Echocardiography, while non-invasive, has limitations in accuracy and operator dependency, which the deep learning model overcomes by integrating comprehensive hemodynamic data and advanced computational techniques **(Figure 15, 16)**.

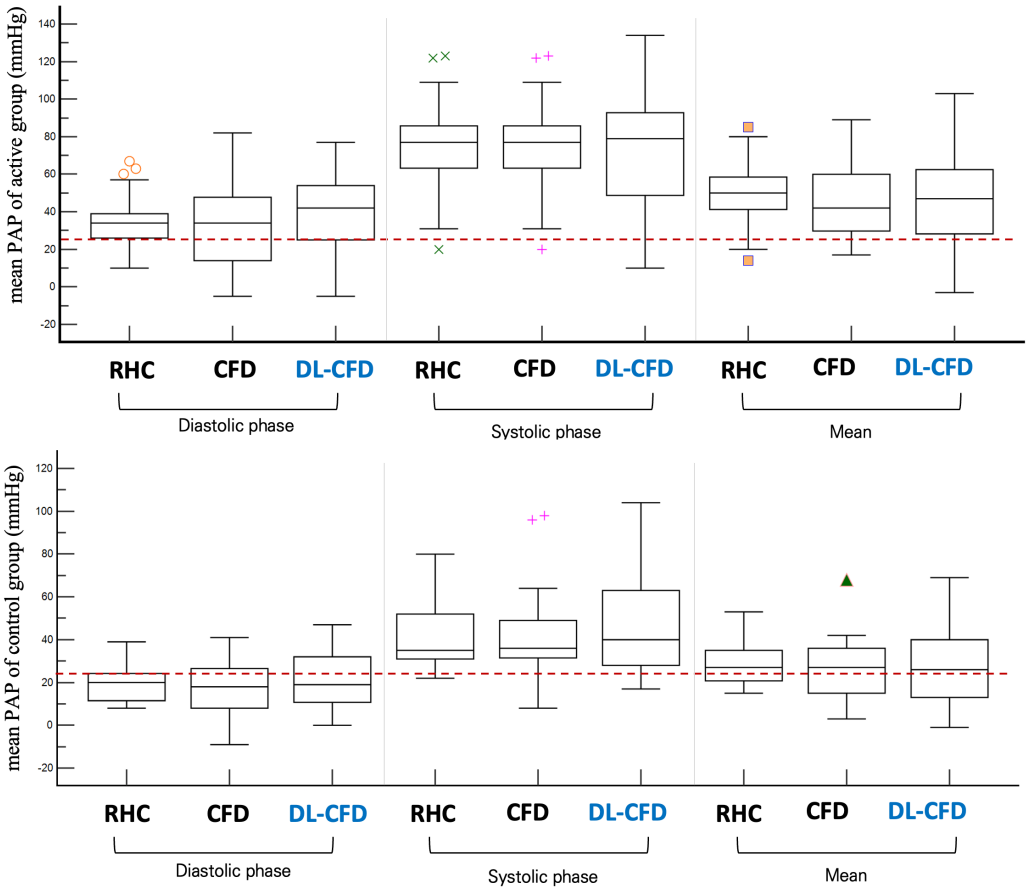

Figure 15. Box plot of mean, systolic, and diastolic PAP values from RHC, CFD simulation, and DL-CFD in PH and non-PH patients.

#	Pressure (image)	Pressure [mmHg]	Pressure range [mmHg]
1		**35.1**	 34.2 36.0
2		**56.5** (Systolic pressure)	 41.5 71.6
3		**63.8**	 58.8 68.8
4	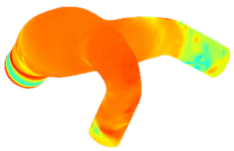	**56.1**	 53.9 58.2
5	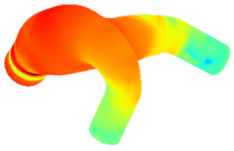	**55.7**	 48.9 62.5
6		**42.9** (Diastolic pressure)	 41.7 44.2

Figure 16. Pressure results according to phase (systolic, diastolic pressure), mPAP, and pressure range.

B. Comparison of Traditional Echocardiography and the Proposed Method

When comparing the correlation between the hemodynamic parameters measured by RHC and the CFD and DL-CFD methods, it is observed that the correlations are lower than those with the traditionally used echocardiography. Specifically, the correlation coefficient between RHC and echocardiography was 0.714 ($p < 0.001$), while the correlation coefficients between RHC and CFD simulation and DL-CFD were 0.543 ($p < 0.001$) and 0.674 ($p < 0.001$), respectively. However, eDL-CFD method showed a higher correlation coefficient of 0.768 ($p < 0.001$) with RHC **(Table 3)**.

Table 3. Correlation coefficients among RHC, echocardiography, CFD simulation, DL-CFD, and eDL-CFD

	RHC	**Echocardio-graphy**	**CFD simulation**	**DL-CFD**	**eDL-CFD**
RHC	-	0.714 ($p < 0.001$)	0.543 ($p < 0.001$)	0.674 ($p < 0.001$)	0.768 ($p < 0.001$)
Echocardio-graphy	0.714 ($p < 0.001$)	-	0.605 ($p < 0.001$)	0.620 ($p < 0.001$)	0.874 ($p < 0.001$)
CFD simulation	0.543 ($p < 0.001$)	0.605 ($p < 0.001$)	-	0.904 ($p < 0.001$)	0.724 ($p < 0.001$)
DL-CFD	0.674 ($p < 0.001$)	0.620 ($p < 0.001$)	0.904 ($p < 0.001$)	-	0.922 ($p < 0.001$)
eDL-CFD	0.768 ($p < 0.001$)	0.874 ($p < 0.001$)	0.724 ($p < 0.001$)	0.922 ($p < 0.001$)	-

DL: deep learning, CFD: computational fluid dynamics, AUC: area under the curve

These results highlight the enhanced diagnostic accuracy of eDL-CFD method over traditional echocardiography. The AUC for the combined method was 98.9%, compared to 94.6% for echocardiography alone, 89.0% for CFD simulation, and 93.0% for DL-CFD.

This demonstrates the potential of the combined approach to serve as a more reliable non-invasive diagnostic tool, improving both sensitivity and specificity in diagnosing PH **(Figure 17)**. This figure illustrates the distribution of predicted PH using various non-invasive techniques, specifically echocardiography, CFD simulation, DL-CFD, and eDL-CFD method in patients with PH confirmed by RHC (mPAP > 25 mmHg).

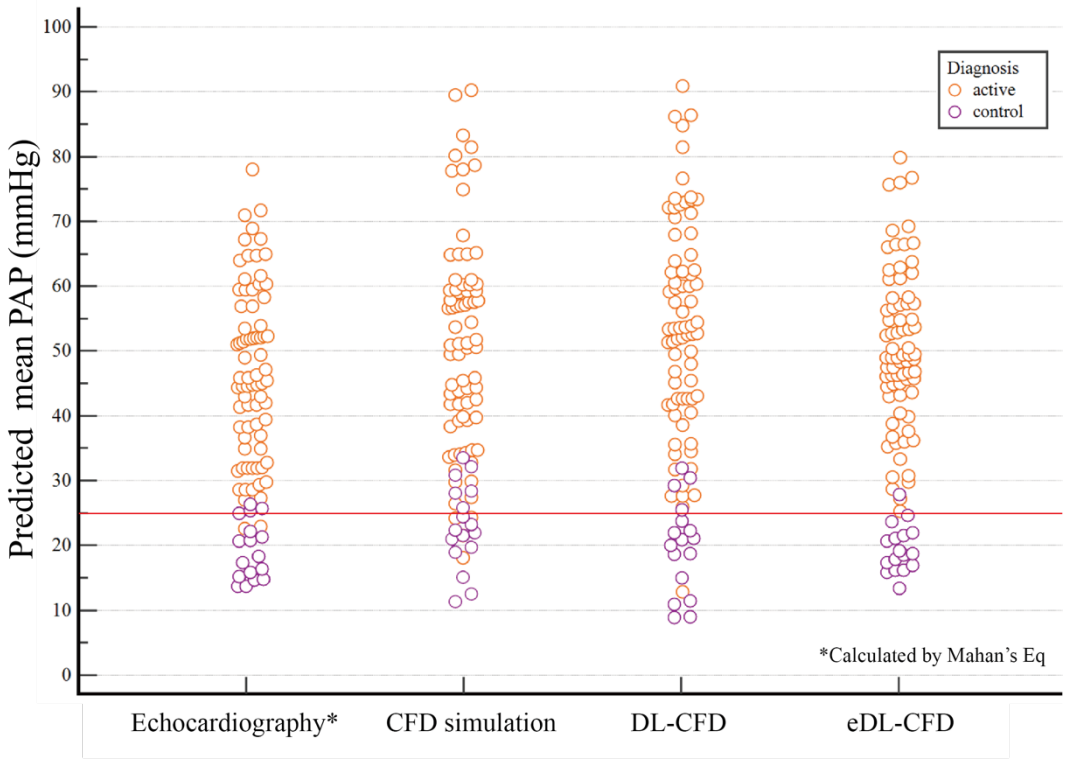

Figure 17. Distribution of predicted PH by non-invasive methods in patients with mPAP > 25 mmHg confirmed by RHC.

Stratified analysis by patient groups revealed significant findings. When the patients were categorized into those with PH (mPAP > 25 mmHg; active group) and those without (mPAP < 25 mmHg; control group), it was observed that many patients who were not diagnosed with PH using echocardiography alone were correctly identified with the eDL-CFD method. This combined approach resulted in an improved specificity of 94.1% compared to 76.4% with echocardiography alone while maintaining a high sensitivity of 97.3% **(Table 4).**

Additionally, the Positive Predictive Value (PPV) and Negative Predictive Value (NPV) for the eDL-CFD method were significantly higher. The PPV for the eDL-CFD method was 94.3%, indicating that a high proportion of patients identified as having PH by this method indeed had the condition. Similarly, the NPV was 97.2%, meaning that nearly all patients identified as not having PH by this method truly did not have the condition. These results show that the eDL-CFD method not only improves sensitivity and specificity but also offers higher PPV and NPV than traditional echocardiography, thus providing a more reliable non-invasive method for PH **(Table 4)**.

Table 4. Diagnostic accuracy of PH patients derived from echocardiography, CFD simulation, DL-CFD and eDL-CFD.

	Sensitivity	Specificity	PPV	NPV	AUC	Accuracy
Echocardiography	97.3%	76.4%	80.5%	96.6%	94.6%	86.9%
CFD simulation	85.0%	75.0%	77.3%	83.3%	89.0%	83.1%
DL-CFD	90.0%	83.3%	84.4%	89.3%	93.0%	84.3%
eDL-CFD	97.3%	94.1%	94.3%	97.2%	98.9%	91.0%

V. DISCUSSION

The relationship between RV-Pulmonary artery coupling and PH is a critical area of focus in the pathophysiology of PH. RV-Pulmonary artery coupling refers to the interaction and synchronization between the RV and the pulmonary artery, which is significantly impacted in PH. As PH progresses, the increased PVR leads to elevated pulmonary artery pressures, placing substantial mechanical stress on the RV. This stress can result in RV hypertrophy and dysfunction, further complicating the management of PH[7, 8].

The integration of eDL-CFD offers several notable clinical benefits, addressing some of the significant challenges in diagnosing and managing PH:

1. Non-Invasive Diagnosis

The eDL-CFD model provides a reliable non-invasive method for diagnosing PH. Traditional diagnostic methods such as RHC are invasive and carry risks of complications. By accurately predicting mPAP through non-invasive imaging techniques like CT and echocardiography, the deep learning model significantly reduces the need for these invasive procedures, thereby improving patient safety and comfort. Additionally, this study examined the correlation between the imaging modalities used (CT, echocardiography), CFD simulation, and RHC. Significant results were observed, confirming the validity of the non-invasive methods in accurately assessing pulmonary hemodynamics. While traditional echocardiography strongly correlates with RHC, the proposed method demonstrates significant correlation and agreement. This indicates that the eDL-CFD approach can be a viable non-invasive alternative for diagnosing PH, potentially offering improved diagnostic accuracy and reliability over traditional echocardiography alone **(Figure 18)** [16, 50-54].

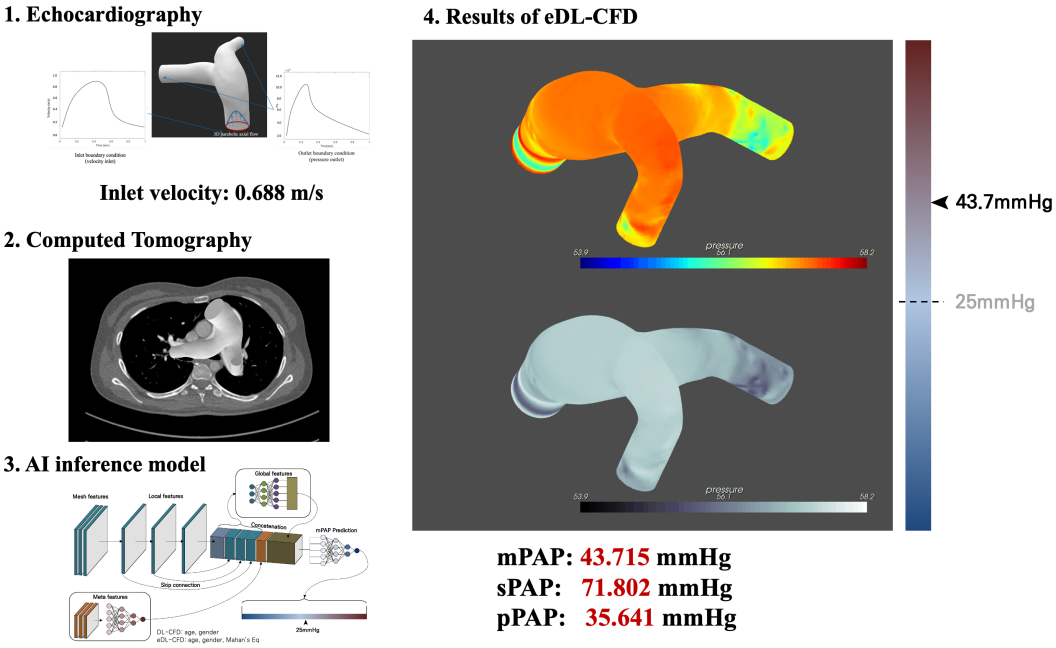

Figure 18. Process and results of eDL-CFD in a PH patient case.

2. Personalized Medicine

One of the standout features of this deep learning model is its ability to incorporate patient-specific data, including anatomical and hemodynamic parameters, to support personalized treatment planning. This capability ensures that each patient receives tailored management strategies based on their unique physiological characteristics, which can improve treatment outcomes and enhance the quality of life for PH patients.

3. Efficiency and Speed

The deep learning model excels in its ability to rapidly analyze and predict hemodynamic parameters. This efficiency is crucial for the timely diagnosis and intervention required in progressive conditions like PH. Quick and accurate diagnostics allow for earlier treatment initiation, which can slow disease progression and improve prognosis.

4. Enhanced Monitoring

The deep learning model facilitates continuous monitoring and assessment of PH patients. By providing real-time insights into the hemodynamic status, the model enables dynamic adjustments to treatment plans, ensuring that therapeutic interventions are always aligned with the current state of the disease. This continuous monitoring capability is particularly beneficial in managing chronic and progressive diseases like PAH, where regular assessment and timely intervention are critical.

Despite the promising results, this study has several limitations that need to be addressed in future research to enhance the model's applicability and robustness:

1. Dataset Size

The current study utilized a relatively small dataset, which may limit the generalizability of the findings. A larger and more diverse dataset would help improve the model's accuracy

and robustness. Future research should focus on incorporating data from a broader patient population, including various demographics and disease severities, to validate the model's effectiveness across different groups.

2. Data Augmentation

Incorporating data augmentation techniques during the training phase can significantly improve the model's ability to handle variability in patient-specific geometries and hemodynamic conditions. Data augmentation methods such as rotation, scaling, and translation can create a more diverse training set, which can help the model generalize better to new, unseen data.

3. Modeling Distal Arteries

To predict wedge pressure more accurately, it is crucial to include detailed representations of the distal sections of the pulmonary arteries in the model. These distal segments play a significant role in the overall hemodynamic profile of the pulmonary circulation. Future models should incorporate this level of detail to enhance the accuracy of wedge pressure predictions, a critical parameter in diagnosing PH.

4. Prospective Clinical Studies

Conducting prospective clinical studies will provide valuable insights into the real-world applicability and impact of the deep learning model on patient outcomes. Such studies can assess the model's performance in clinical settings, evaluate its integration with existing diagnostic workflows, and determine its overall effectiveness in improving patient care. These studies are essential for validating the model's clinical utility and ensuring that it meets the needs of healthcare providers and patients.

In summary, the integration of eDL-CFD represents a significant advancement in the non-invasive diagnosis and management of PH. This study demonstrates the potential of

the deep learning model to provide accurate, patient-specific predictions of hemodynamic parameters, thereby offering a viable alternative to traditional invasive diagnostic methods. The model's ability to facilitate personalized medicine, enhance diagnostic efficiency, and enable continuous monitoring underscores its potential to improve clinical outcomes for PH patients.

Future research should focus on expanding the dataset, incorporating data augmentation techniques, and refining the model to include distal arterial segments. Prospective clinical studies will be crucial in validating the model's effectiveness in real-world settings and ensuring its seamless integration into clinical practice. By addressing these areas, we can further enhance the model's predictive capabilities and clinical applicability, ultimately leading to better patient care and outcomes in PH management.

VI. CONCLUSION

In this study, we developed a non-invasive, rapid diagnostic model for PH using eDL-CFD based on CT and echocardiography data. The proposed method demonstrated high accuracy in predicting mPAP, offering a viable alternative to the current gold standard of RHC. The integration of patient-specific geometric and hemodynamic data with advanced deep learning algorithms holds significant promise for improving PH diagnosis and treatment planning, ultimately leading to better patient outcomes. Our comparative analysis revealed that while traditional echocardiography strongly correlates with RHC, the eDL-CFD method shows significant correlation and agreement. This indicates that the eDL-CFD approach can be a viable non-invasive alternative for diagnosing PH, potentially offering improved diagnostic accuracy and reliability over traditional echocardiography alone.

By continuing to refine this technology and incorporating larger datasets, we aim to further enhance its diagnostic precision and clinical applicability. This approach represents a significant advancement in the field of medical imaging and computational diagnostics, providing a robust framework for the non-invasive assessment and management of PH.

REFERENCES

[1] McLaughlin VV, McGoon MD. Pulmonary arterial hypertension. Circulation. 2006;114(13):1417-31.

[2] Farber HW, Loscalzo J. Pulmonary arterial hypertension. New England Journal of Medicine. 2004;351(16):1655-65.

[3] Humbert M, Sitbon O, Simonneau G. Treatment of pulmonary arterial hypertension. New England Journal of Medicine. 2004;351(14):1425-36.

[4] Simonneau G, Gatzoulis MA, Adatia I, Celermajer D, Denton C, Ghofrani A, et al. Updated clinical classification of pulmonary hypertension. Turk Kardiyoloji Dernegi arsivi: Turk Kardiyoloji Derneginin yayin organidir. 2014;42:45-54.

[5] Hoeper MM, Bogaard HJ, Condliffe R, Frantz R, Khanna D, Kurzyna M, et al. Definitions and diagnosis of pulmonary hypertension. Journal of the American College of Cardiology. 2013;62(25S):D42-D50.

[6] Vonk-Noordegraaf A, Haddad F, Chin KM, Forfia PR, Kawut SM, Lumens J, et al. Right heart adaptation to pulmonary arterial hypertension: physiology and pathobiology. Journal of the American College of Cardiology. 2013;62(25S):D22-D33.

[7] Richter MJ, Peters D, Ghofrani HA, Naeije R, Roller F, Sommer N, et al. Evaluation and prognostic relevance of right ventricular–arterial coupling in pulmonary hypertension. American journal of respiratory and critical care medicine. 2020;201(1):116-9.

[8] Hsu S, Simpson CE, Houston BA, Wand A, Sato T, Kolb TM, et al. Multi-beat right ventricular-arterial coupling predicts clinical worsening in pulmonary arterial hypertension. Journal of the American Heart Association. 2020;9(10):e016031.

[9] Peacock A, Murphy N, McMurray J, Caballero L, Stewart S. An epidemiological study of pulmonary arterial hypertension. European Respiratory Journal. 2007;30(1):104-9.

[10] Ling Y, Johnson MK, Kiely DG, Condliffe R, Elliot CA, Gibbs JSR, et al. Changing demographics, epidemiology, and survival of incident pulmonary arterial hypertension: results from the pulmonary hypertension registry of the United Kingdom and Ireland. American journal of respiratory and critical care medicine. 2012;186(8):790-6.

[11] Badesch DB, Raskob GE, Elliott CG, Krichman AM, Farber HW, Frost AE, et al. Pulmonary arterial hypertension: baseline characteristics from the REVEAL Registry. Chest. 2010;137(2):376-87.

[12] Humbert M, Sitbon O, Chaouat A, Bertocchi M, Habib G, Gressin V, et al. Pulmonary arterial hypertension in France: results from a national registry. American journal of respiratory and critical care medicine. 2006;173(9):1023-30.

[13] Galiè N, Barberà JA, Frost AE, Ghofrani H-A, Hoeper MM, McLaughlin VV, et al. Initial use of ambrisentan plus tadalafil in pulmonary arterial hypertension. New England Journal of Medicine. 2015;373(9):834-44.

[14] McLaughlin VV, Hoeper MM, Channick RN, Chin KM, Delcroix M, Gaine S, et al. Pulmonary arterial hypertension-related morbidity is prognostic for mortality. Journal of the American College of Cardiology. 2018;71(7):752-63.

[15] Humbert M, Kovacs G, Hoeper MM, Badagliacca R, Berger RM, Brida M, et al. 2022 ESC/ERS Guidelines for the diagnosis and treatment of pulmonary hypertension: Developed by the task force for the diagnosis and treatment of pulmonary hypertension of the European Society of Cardiology (ESC) and the European Respiratory Society (ERS). Endorsed by the International Society for Heart and Lung Transplantation (ISHLT) and the European Reference Network on rare respiratory diseases (ERN-LUNG). European heart journal. 2022;43(38):3618-731.

[16] Fisher MR, Forfia PR, Chamera E, Housten-Harris T, Champion HC, Girgis RE, et al. Accuracy of Doppler echocardiography in the hemodynamic assessment of pulmonary hypertension. American journal of respiratory and critical care medicine. 2009;179(7):615-21.

[17] Rudski LG, Lai WW, Afilalo J, Hua L, Handschumacher MD, Chandrasekaran K, et al. Guidelines for the echocardiographic assessment of the right heart in adults: a report from the American Society of Echocardiography: endorsed by the European Association of Echocardiography, a registered branch of the European Society of Cardiology, and the Canadian Society of Echocardiography. Journal of the American society of echocardiography. 2010;23(7):685-713.

[18] Lee S-E, Im JH, Sung JM, Cho I-J, Shim CY, Hong G-R, et al. Detection of mechanical complications related to the potential risk of sudden cardiac death in patients with pulmonary arterial hypertension by computed tomography. International Journal of Cardiology. 2017;243:460-5.

[19] Grosse C, Grosse A. CT findings in diseases associated with pulmonary hypertension: a current review. Radiographics. 2010;30(7):1753-77.

[20] Rajaram S, Swift AJ, Capener D, Elliot CA, Condliffe R, Davies C, et al. Comparison of the diagnostic utility of cardiac magnetic resonance imaging, computed tomography, and echocardiography in assessment of suspected pulmonary arterial hypertension in patients with connective tissue disease. The Journal of rheumatology. 2012;39(6):1265-74.

[21] McGoon MD, Benza RL, Escribano-Subias P, Jiang X, Miller DP, Peacock AJ, et al. Pulmonary arterial hypertension: epidemiology and registries. Journal of the American College of Cardiology. 2013;62(25S):D51-D9.

[22] Members WC, McLaughlin VV, Archer SL, Badesch DB, Barst RJ, Farber HW, et al. ACCF/AHA 2009 expert consensus document on pulmonary hypertension: a report of the American College of Cardiology Foundation task force on expert consensus documents and the American Heart Association: developed in collaboration with the American College of Chest Physicians, American Thoracic Society, Inc., and the Pulmonary Hypertension Association. Circulation. 2009;119(16):2250-94.

[23] Rich S, Dantzker DR, Ayres SM, Bergofsky EH, Brundage BH, Detre KM, et al. Primary pulmonary hypertension: a national prospective study. Annals of internal medicine. 1987;107(2):216-23.

[24] Taylor CA, Figueroa C. Patient-specific modeling of cardiovascular mechanics. Annual review of biomedical engineering. 2009;11:109-34.

[25] Balossino R, Gervaso F, Migliavacca F, Dubini G. Effects of different stent designs on local hemodynamics in stented arteries. Journal of biomechanics. 2008;41(5):1053-61.

[26] Ku DN. Blood flow in arteries. Annual review of fluid mechanics. 1997;29(1):399-434.

[27] Gallo D, Steinman DA, Bijari PB, Morbiducci U. Helical flow in carotid bifurcation as surrogate marker of exposure to disturbed shear. Journal of biomechanics. 2012;45(14):2398-404.

[28] Morris PD, Narracott A, von Tengg-Kobligk H, Soto DAS, Hsiao S, Lungu A, et al. Computational fluid dynamics modelling in cardiovascular medicine. Heart. 2016;102(1):18-28.

[29] Li M, Beech-Brandt J, John L, Hoskins P, Easson W. Numerical analysis of pulsatile blood flow and vessel wall mechanics in different degrees of stenoses. Journal of biomechanics. 2007;40(16):3715-24.

[30] Chnafa C, Mendez S, Nicoud F. Image-based simulations show important flow fluctuations in a normal left ventricle: what could be the implications? Annals of biomedical engineering. 2016;44:3346-58.

[31] Tang BT, Cheng CP, Draney MT, Wilson NM, Tsao PS, Herfkens RJ, et al. Abdominal aortic hemodynamics in young healthy adults at rest and during lower limb exercise: quantification using image-based computer modeling. American Journal of Physiology-Heart and Circulatory Physiology. 2006;291(2):H668-H76.

[32] Van de Vosse FN, Stergiopulos N. Pulse wave propagation in the arterial tree. Annual Review of Fluid Mechanics. 2011;43:467-99.

[33] Litjens G, Kooi T, Bejnordi BE, Setio AAA, Ciompi F, Ghafoorian M, et al. A survey on deep learning in medical image analysis. Medical image analysis. 2017;42:60-88.

[34] Esteva A, Kuprel B, Novoa RA, Ko J, Swetter SM, Blau HM, et al. Dermatologist-level classification of skin cancer with deep neural networks. nature. 2017;542(7639):115-8.

[35] Gulshan V, Peng L, Coram M, Stumpe MC, Wu D, Narayanaswamy A, et al. Development and validation of a deep learning algorithm for detection of diabetic retinopathy in retinal fundus photographs. jama. 2016;316(22):2402-10.

[36] Rajpurkar P, Irvin J, Zhu K, Yang B, Mehta H, Duan T, et al. Chexnet: Radiologist-level pneumonia detection on chest x-rays with deep learning. arXiv preprint arXiv:171105225. 2017.

[37] Litjens G, Sánchez CI, Timofeeva N, Hermsen M, Nagtegaal I, Kovacs I, et al. Deep learning as a tool for increased accuracy and efficiency of histopathological diagnosis. Scientific reports. 2016;6(1):26286.

[38] Huang S-C, Pareek A, Seyyedi S, Banerjee I, Lungren MP. Fusion of medical imaging and electronic health records using deep learning: a systematic review and implementation guidelines. NPJ digital medicine. 2020;3(1):136.

[39] Chen H, Zhang Y, Kalra MK, Lin F, Chen Y, Liao P, et al. Low-dose CT with a residual encoder-decoder convolutional neural network. IEEE transactions on medical imaging. 2017;36(12):2524-35.

[40] Lau EM, Manes A, Celermajer DS, Galie N. Early detection of pulmonary vascular disease in pulmonary arterial hypertension: time to move forward. European heart journal. 2011;32(20):2489-98.

[41] Guo Z, Li X, Huang H, Guo N, Li Q. Deep learning-based image segmentation on multimodal medical imaging. IEEE Transactions on Radiation and Plasma Medical Sciences. 2019;3(2):162-9.

[42] Zhang Z, Xie Y, Xing F, McGough M, Yang L, editors. Mdnet: A semantically and visually interpretable medical image diagnosis network. Proceedings of the IEEE conference on computer vision and pattern recognition; 2017.

[43] Hinton G. Deep learning—a technology with the potential to transform health care. Jama. 2018;320(11):1101-2.

[44] Xie Y, Zhang J, Xia Y, Fulham M, Zhang Y. Fusing texture, shape and deep model-learned information at decision level for automated classification of lung nodules on chest CT. Information Fusion. 2018;42:102-10.

[45] Raissi M, Perdikaris P, Karniadakis GE. Physics-informed neural networks: A deep learning framework for solving forward and inverse problems involving nonlinear partial differential equations. Journal of Computational physics. 2019;378:686-707.

[46] Raissi M, Yazdani A, Karniadakis GE. Hidden fluid mechanics: Learning velocity and pressure fields from flow visualizations. Science. 2020;367(6481):1026-30.

[47] Chen Y, Lu L, Karniadakis GE, Dal Negro L. Physics-informed neural networks for inverse problems in nano-optics and metamaterials. Optics express. 2020;28(8):11618-33.

[48] Cheng J-Z, Ni D, Chou Y-H, Qin J, Tiu C-M, Chang Y-C, et al. Computer-aided diagnosis with deep learning architecture: applications to breast lesions in US images and pulmonary nodules in CT scans. Scientific reports. 2016;6(1):24454.

[49] Lee J-G, Jun S, Cho Y-W, Lee H, Kim GB, Seo JB, et al. Deep learning in medical imaging: general overview. Korean journal of radiology. 2017;18(4):570.

[50] Tsubata H, Nakanishi N, Itatani K, Takigami M, Matsubara Y, Ogo T, et al. Pulmonary artery blood flow dynamics in chronic thromboembolic pulmonary hypertension. Scientific Reports. 2023;13(1):6490.

[51] Tang BT, Pickard SS, Chan FP, Tsao PS, Taylor CA, Feinstein JA. Wall shear stress is decreased in the pulmonary arteries of patients with pulmonary arterial hypertension: an image-based, computational fluid dynamics study. Pulmonary circulation. 2012;2(4):470-6.

[52] Janda S, Shahidi N, Gin K, Swiston J. Diagnostic accuracy of echocardiography for pulmonary hypertension: a systematic review and meta-analysis. Heart. 2011;97(8):612-22.

[53] Alhamad EH, Al-Boukai AA, Al-Kassimi FA, Alfaleh HF, Alshamiri MQ, Alzeer AH, et al. Prediction of pulmonary hypertension in patients with or without interstitial lung disease: reliability of CT findings. Radiology. 2011;260(3):875-83.

[54] Ley S, Ley-Zaporozhan J, Pitton MB, Schneider J, Wirth GM, Mayer E, et al. Diagnostic performance of state-of-the-art imaging techniques for morphological assessment of vascular abnormalities in patients with chronic thromboembolic pulmonary hypertension (CTEPH). European radiology. 2012;22:607-16.

ABSTRACT IN KOREAN

폐고혈압 환자의 진단 · 치료 예후예측을 위한 의료영상기반 예측모델 개발과 유효성 검증

<지도교수 장혁재>

연세대학교 대학원 생체공학협동과정

하성민

폐고혈압(pulmonary hypertension, PH)은 폐동맥 압력이 비정상적으로 상승하여 심장과 폐에 과도한 부담을 주며, 치료하지 않으면 심부전 등의 심각한 건강 문제를 초래할 수 있는 질환이다. 일반적으로 폐고혈압 검사는 우심도자술(right heart catheterization, RHC)이 표준 진단법(gold standard)이나, 침습검사로 환자에게 부담이 있을 수 있다. 반면, 비침습검사인 심초음파는 초기 스크리닝 도구로 유용하지만, 진단 정확도가 우심도자술에 비해 낮은 상황이다. 따라서 본 연구는 심초음파(echocardiography)와 컴퓨터 단층촬영(computed tomography, CT)으로 혈역학적 유체 역학(computational fluid dynamics, CFD) 시뮬레이션 결과를 도출하고, 이러한 결과를 이용해 딥러닝 모델(deep learning with CFD simulation, DL-CFD) 및 심초음파의 임상 결과를 포함한 모델(echocardiography + DL-CFD, eDL-CFD)을 개발하고 유효성을 평가하였다. 2008 년부터 2019 년까지, PH 평가를 위해 우심도자술(RHC)을 받은 92 명의 환자를 대상으로 후향적 연구를 수행하였다. 이 중 75 명은 PH 로 진단되었고(평균 폐동맥압; mean pulmonary arterial pressure, mPAP > 25 mmHg), 17 명은 정상군이다 (mPAP < 25 mmHg). 비교 분석 결과, RHC 와 개발된 CFD 및 DL-CFD 방법 간의 상관관계는 전통적인

심초음파보다 낮았으나, eDL-CFD 방법은 RHC 와 더 높은 상관관계를 보였다. eDL-CFD 방법의 AUC 는 98.9%로, 심초음파 단독(94.6%)보다 높은 결과를 보였고, 특이도가 76.4%에서 94.1%로 향상되었으며, 민감도는 97.3%로 유지되었다. 이 결과 eDL-CFD 접근법이 심초음파 단독검사 보다 개선된 진단 정확도와 신뢰성을 제공할 수 있는 유효한 비침습적 대안임을 보였다. 또한 본 연구는 비침습적인 방법으로 개인 맞춤형 치료 계획 및 질병 진행에 대한 예측 가능성을 확인하였다. 향후 연구는 다양한 데이터셋을 활용하고 데이터 증강 기법을 적용하여 모델의 일반화 가능성과 정확성을 더욱 향상시키는 데 초점을 맞출 것이다.

핵심되는 말 : 폐고혈압, 혈류역학, 딥러닝, 전산 유체 역학, 비침습적 진단